



Technical Note

New Methodology for Intertidal Seaweed Biomass Estimation Using Multispectral Data Obtained with Unoccupied Aerial Vehicles

Débora Borges ^{1,*} , Lia Duarte ² , Isabel Costa ¹, Ana Bio ¹ , Joelen Silva ¹, Isabel Sousa-Pinto ^{1,3} and José Alberto Gonçalves ^{1,2}

¹ Interdisciplinary Centre of Marine and Environmental Research (CIIMAR/CIMAR), University of Porto, 4450-208 Matosinhos, Portugal

² Department of Geosciences Environment and Spatial Planning, Faculty of Sciences, University of Porto, 4200-319 Porto, Portugal

³ Department of Biology, Faculty of Sciences, University of Porto, 4200-319 Porto, Portugal

* Correspondence: debora.borges@ciimar.up.pt

Abstract: Seaweed assemblages include a variety of structuring species providing habitats, food and shelter for organisms from different trophic levels. Monitoring intertidal seaweed traditionally involves targeting small areas to collect data on species' biological traits, which is often labour intensive and covers only a small area of the rocky reef under study. Given the various applications for seaweeds and their compounds, there has been an increase in demand for biomass triggered by the development of new markets. Such biomass demand generates new challenges for biomass quantification and the definition of future in-take harvesting commercial quotas by regulating agencies. The use of Unoccupied Aerial Vehicles (UAVs) as a low-cost yet efficient monitoring solution, combined with new sensors such as multispectral cameras, has been proposed for mapping intertidal reefs and seaweed in particular. In this study, a new methodology was developed and validated to quantify intertidal seaweed biomass based on multispectral UAV imagery, which was made available through an easy-to-use QGIS plugin (named SWUAV_BIO) that automates such biomass estimation. This tool was applied to a case study where the standing stock of *Fucus* spp. beds located at Viana do Castelo rocky shore (northern Portugal) was assessed using UAV multispectral imagery, providing a reference for future UAV-based ecological studies. Although comparison with the in situ assessments showed that biomass was underestimated by 36%, the SWUAV_BIO plugin is a valuable tool, as it provides an expedited (albeit conservative) seaweed standing stock assessment that can be used to monitor seaweed populations, their changes, and assess the effect of harvesting. These data can be used for an informed and sustainable management of seaweed resources by the competent authorities.



Citation: Borges, D.; Duarte, L.; Costa, I.; Bio, A.; Silva, J.; Sousa-Pinto, I.; Gonçalves, J.A. New Methodology for Intertidal Seaweed Biomass Estimation Using Multispectral Data Obtained with Unoccupied Aerial Vehicles. *Remote Sens.* **2023**, *15*, 3359. <https://doi.org/10.3390/rs15133359>

Academic Editors: Javier Leon, Daniel L. Harris and Stephanie Duce

Received: 17 May 2023

Revised: 27 June 2023

Accepted: 28 June 2023

Published: 30 June 2023



Copyright: © 2023 by the authors. Licensee MDPI, Basel, Switzerland. This article is an open access article distributed under the terms and conditions of the Creative Commons Attribution (CC BY) license (<https://creativecommons.org/licenses/by/4.0/>).

Keywords: supervised classification; normalized difference vegetation index; QGIS plugin; accuracy

1. Introduction

Seaweed assemblages are essential to coastal environments as they include a variety of structuring species providing habitats, food and shelter for organisms from different trophic levels and supporting complex trophic webs. Seaweeds are also a natural resource for human use, and an increased demand for biomass has been triggered by the development of new markets, namely in the food and health sectors. They are presently considered a healthy food and a rich source of bioactive compounds [1,2] and thus a valuable ingredient for biomedical, nutraceutical and cosmeceutical products [3,4]. Such biomass demand can act as an additional pressure on coastal environments, particularly for intertidal areas, which are easily accessed by foot and, therefore, more susceptible to seaweed harvesting and trampling.

Monitoring intertidal seaweed assemblages traditionally involves targeting patchy areas of the rocky reefs using quadrats, along transects or not, and collecting data on species' biological traits [5,6]. These methods are labour intensive and cover only a small area of the rocky reef under study due to time/tide constraints (e.g., see [7,8]). In recent years, the application of Unoccupied Aerial Vehicles (UAVs) as a low-cost yet efficient monitoring solution has increased in several contexts. New sensors that can be mounted on UAVs have been developed, providing new tools for research implementation. Such is the case with multispectral cameras, which have become widely used in agriculture [9–11] and viticulture [12,13] to assess crop health and maturation but also crop biomass (e.g., [14]). Coastal studies have also benefited from such advances, and several UAV-based multispectral methodologies and workflows have been proposed for mapping intertidal reefs [15,16] and seaweed in particular [17–21]. For kelp, workflows, including the calculation of simple vegetation indices from RGB imagery, have been developed to classify kelp canopy as a binary presence/absence layer, and to discriminate these organisms from the surrounding background (see [22–24]).

However, few studies have been able to remotely estimate the biomass of intertidal seaweeds (e.g., see [25,26]). The latest study applied multispectral UAV aerial photography data to evaluate the biomass of seaweed in an intertidal zone that were later processed through the use of machine learning algorithms [26]. However, most studies that have used multispectral data to access seaweed biomass were performed on cultivated land-based [27] or open-sea systems [28] and also on floating algal blooms [29]. Such studies rely on the calculation of vegetation indexes using the available bands from multispectral sensors. One of the most used indexes is the Normalized Difference Vegetation Index (NDVI), which relates to red and near-Infrared (NIR) bands and has proven to successfully map seaweed biomass at different scales (see [25,30]).

NDVI was initially developed to quantify terrestrial vegetation density and health from aerial images [31–33]. It utilizes the characteristic increased reflectance in the NIR region (due to tissular/cellular structures) and decreased reflectance in the red regions of the electromagnetic spectrum (due to chlorophyll absorption) exhibited by vegetation [34,35]. NDVI ranges from -1 to $+1$, with values around and below zero indicating relatively low amounts of vegetation [25]. Seaweeds have diverse morphology, water content, cellular structures and pigments, presenting chlorophylls as common photosynthetic pigments [36]. Due to the fact that it is related to the chlorophyll content, NDVI can therefore be used as a proxy for seaweed biomass.

Remote sensing data are normally analysed using specific software packages. Geographical Information System (GIS) software packages also include modules for remote sensing data processing and analysis in their raster processing tools. Within the open-source domain, QGIS, which is a modular software package to which users can contribute modules designated as plugins, can be used for the analysis of remote sensing data. In the particular field of image classification, a specific plugin, designated Semi-Automatic Classification Plugin (SCP), developed by Luca Congedo, has been available since 2012 [37]. It has become very popular for satellite remote sensing image processing, for example, in forestry [38], but has also been recently used to process UAV multispectral imagery, also in vegetation analysis, including imagery from coastal areas, such as marshes and dunes (see [39–41]).

However, to our knowledge, the present study is the first that integrates GIS and image classification to estimate the biomass of intertidal seaweeds using remotely-sensed imagery, and there are no macros or plugins within image data processing software that implement such methodologies for an expedited standing stock assessment that can help authorities to set harvesting limits and sustainably manage intertidal seaweed resources.

The primary objective of this study was to develop and validate a methodology to quantify the intertidal seaweed biomass based on multispectral imagery acquired with a UAV and make it freely available through an easy-to-use QGIS plugin (named SWUAV_BIO plugin) that automates such biomass estimation. A secondary objective was to apply this

tool to a case study and determine *Fucus* spp. total biomass, thus providing a reference for future UAV-based ecological studies.

The methodology was embedded as a plugin in the QGIS software, making use of the SCP plugin, which has the advantage of being integrated with several other geoprocessing tools. The species selected for the study were *Ulva* spp., *Codium* spp., *Chondrus crispus*, *Osmundea pinnatifida*, *Fucus* spp. and *Laminaria ochroleuca*, given their conspicuous abundance in the northwest coast of Portugal and their current or potential commercial use.

2. Materials and Methods

The conception, design, and implementation of the methodology to quantify intertidal seaweed biomass based on multispectral UAV imagery followed the sequential steps described in the following sections and summarised below (Figure 1): (1) seaweed species-based NDVI/biomass relationship parametrization; (2) the integration of the obtained equations in the SWUAV_BIO plugin to automate the process; (3) plugin methodology validation comparing (a) in situ biomass of *Fucus* spp., based on percentage cover field data with (b) NDVI-based *Fucus* spp. UAV-imagery biomass assessment (using the SWUAV_BIO plugin); and (4) a case study with the SWUAV_BIO application in a different context.

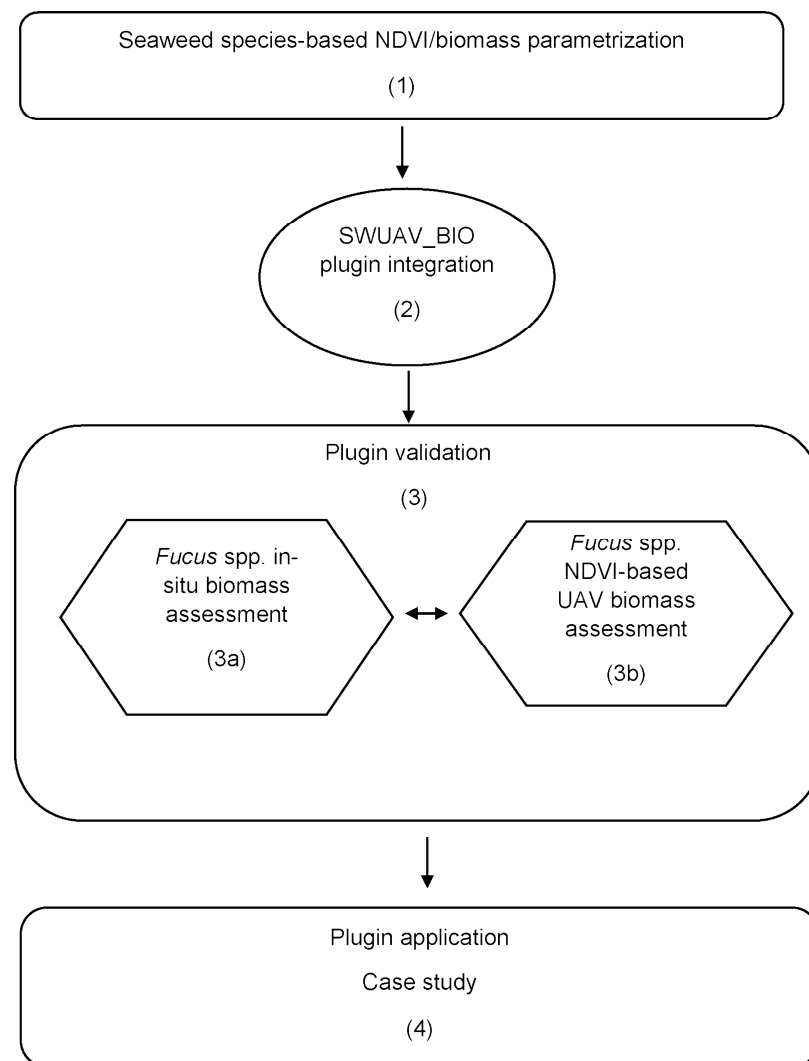


Figure 1. Workflow for the conception, design and implementation of the methodology to quantify intertidal seaweed biomass based on multispectral Unoccupied Aerial Vehicles (UAVs) imagery. Information between brackets is referred to in the main text.

2.1. Seaweed Species-Based NDVI/Biomass Relationship

In order to relate the NDVI (calculated as $(\text{RNIR}-\text{RRed})/(\text{RNIR}+\text{RRed})$, where R refers to reflectance) to the biomass of the intertidal seaweed, the relationship between these variables was assessed based on the reflectance data collected in the field with a handheld spectrometer (ASD HandHeld 2, Malvern Panalytical, Malvern, UK). In the field, seaweeds were grouped according to their accessory pigments, which are responsible for their colour, and reflectance readings were performed in terms of species or genera (for those species with dubious in situ discrimination). The species studied were *Ulva* spp. and *Codium* spp. (green seaweeds), *Chondrus crispus* and *Osmundea pinnatifida* (red seaweeds), and *Laminaria ochroleuca* and *Fucus* spp. (brown seaweeds).

The procedure consisted of the experimental addition and removal of seaweed blades to and from a 0.023 m² black surface matching the spectrometer Ground Field of View (GFOV). The reflectance spectra were collected every 1 nm over 325–1075 nm, and, for each sample, ten readings were taken and subsequently averaged to create a single spectral profile. A white reference panel was used before each measurement as a 100% reflectance standard. The spectrometer was calibrated before the initial measurement and after every ten readings. The measurements ranged from one single blade to overfilling the GFOV with seaweed blades, progressively adding several layers following the methodology described by [42] for seagrass. Seaweed samples were subsequently bagged and transported to the laboratory to be dried at 60 °C for 48 h and weighed to obtain the respective dry weight (DW). The data from the spectrometer were retrieved and stored using RS3 software (Malvern Panalytical, Malvern, UK) and then converted to reflectance units using ViewSpec Pro software (Malvern Panalytical, Malvern, UK). Subsequently, reflectance data were imported to Excel (Microsoft, Washington, DC, USA) for further analysis. To ensure that the NDVI readings obtained with the spectrometer were related to those obtained with the UAV-mounted multispectral camera, the same wavelength ranges for the NIR (840 +/− 20 nm) and Red (668 +/− 5 nm) bands were used for the NDVI calculations. Before computing the NDVI, an average of the reflectance for each corresponding wavelength range was calculated.

2.2. Plugin Design

A GIS open-source plugin was developed in QGIS [43], an intuitive and user-friendly open-source and free GIS software complemented by several algorithms from other external software, such as the System for Automated Geoscientific Analyses (SAGA), Geographic Resources Analysis Support System (GRASS) and Geospatial Data Abstraction Library (GDAL) [44–46]. The new SWUAV_BIO plugin was developed using Python, an open-source programming language [47], and the *Plugin Builder* combined with the *Qt Designer* framework to create the graphical interface and several libraries, such as PyQt Application Programming Interface (API) and QGIS API [48,49], to develop the code.

The plugin is composed of five sections: (1) the input section, where the user can open the input files for the study; (2) the seaweed species section, where the user chooses the seaweed species to study, considering the three seaweed groups (*Red Seaweed*, *Green Seaweed* and *Brown Seaweed*); (3) the biomass estimation equations section, where the user defines the equation to estimate the biomass (using a pre-defined or introduced equation); (4) the output section, where the user should define the output directories to allocate a biomass raster and an html page with the statistics about the biomass areas; and (5), the preview study zone section, where the input information is presented and the user can define the study zone through a manually drawn polygon.

The SWUAV_BIO plugin (workflow summarised in Figure 2) requires two main inputs: the classified image (in which one of the classes corresponds to the seaweed, which should be identified in the *Attribute to isolate* combo box) and the NDVI map. These input files have to be previously created with appropriate software such as QGIS (used here) or, for instance, ArcGIS, ENVI or R.

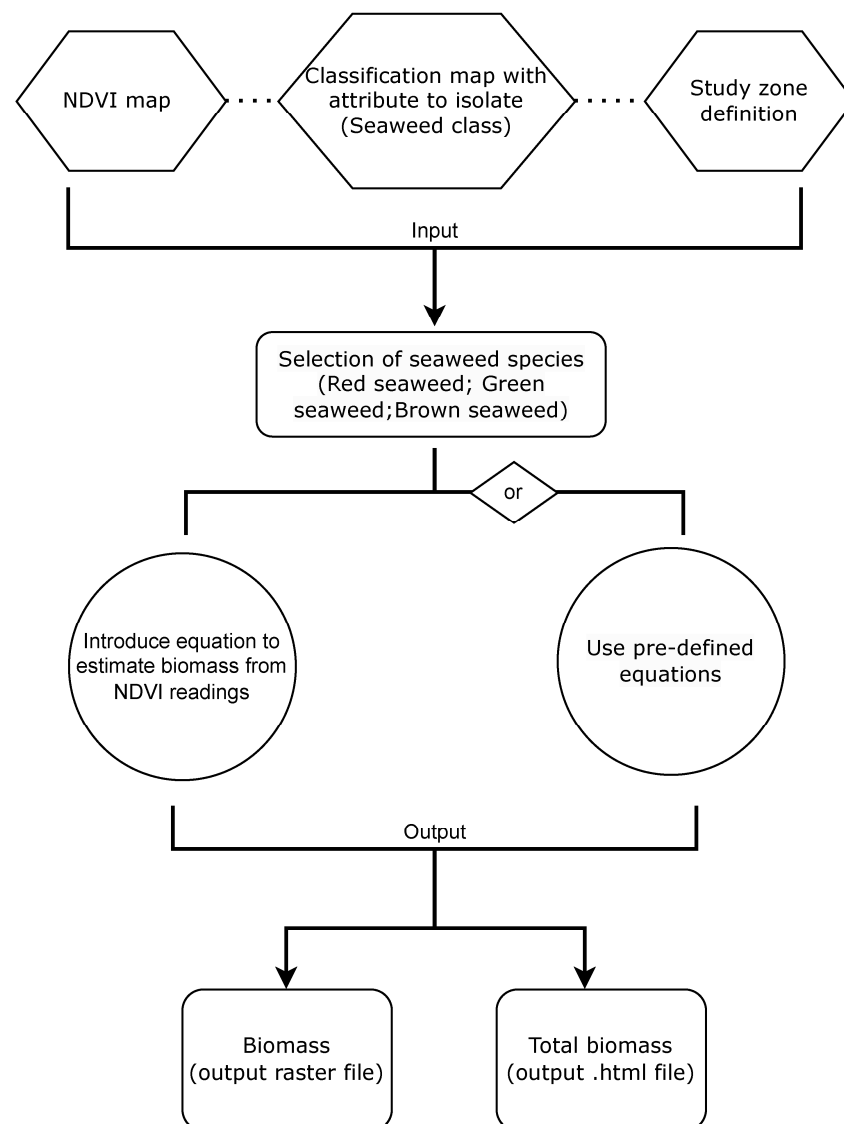


Figure 2. SWUAV_BIO plugin summarised workflow.

The equations relating the NDVI to the species' biomass (developed as described above) were integrated in the SWUAV_BIO plugin. Since the validation of the equations was only performed for *Fucus* spp. (Section 2.3), the validation status (validated or not validated) is indicated in brackets after the species name in the plugin when selecting the species to apply a pre-defined equation. The user may (1) use the pre-defined equation, selecting *Use pre-defined equations*, or (2) introduce a new equation, selecting *Introduce manually the equation to estimate biomass*. The SWUAV_BIO plugin returns two different outputs: (1) a raster with the biomass (g DWm^{-2}) estimation and (2) an html file with the statistical values of the biomass raster where the *Sum* variable (referring to the sum of cell values), represents the total biomass or standing stock (g DW) for the defined study area. The plugin is free and open source and available on the GitHub platform (https://github.com/swuavproject/swuav_plugin, accessed on 31 October 2021). A tutorial is also provided in GitHub, to help the users.

2.3. Plugin Validation

The plugin was validated by assessing the biomass from a *Fucus* spp. bed using field observations and multispectral UAV surveys of an intertidal area on the NW coast of Portugal, as described below.

2.3.1. Study Area

The study area was located on the rocky shore of Vila Chã (41°17'43.4"N, 8°44'13.2"W) in Northern Portugal. This area has a diversified cover with sandy patches and rocky outcrops, colonized with diverse seaweeds, mussels (*Mytilus* spp.), barnacles (*Chthamalus* spp.) and limpets, among others, (*Patella* spp.), following the zonation patterns described for temperate reefs [15]. In the centre of the main rocky outcrop, a relatively sheltered area, there are some isolated beds of *Fucus* spp. (brown seaweed) that are exposed during low tide, which were used for SWUAV_BIO plugin validation.

2.3.2. In Situ Data Collection

The field work took place on 17 December 2020, during low tide, in order to collect data on the percentage cover of *Fucus* spp. beds and to perform an RGB and multispectral UAV flight over those beds. Percentage cover field data were gathered using a sampling unit (quadrat) of 50 × 50 cm divided into 25 sub-quadrats of 10 × 10 cm (each representing 4% of the total area). Ten georeferenced quadrats were haphazardly placed on the *Fucus* spp. beds, and the percentage cover was recorded, as well as the bare substrate. In order to build a predictive equation for *Fucus* spp. relating the percentage cover and the biomass, 32 random samples from the same shore, corresponding to a wide range of percentage cover per sampling unit (5–53%), had been previously collected (on a different day), dried and weighed in the laboratory, obtaining DW values for different cover percentages. To assess the fitness of the equation, the R^2 and the residuals, e_i , were calculated, the latter being the difference between measured and estimated values. The Root Mean Square Error (RMSE) was calculated according to expression (1):

$$RMSE = \sqrt{\frac{1}{n} \sum_i^n e_i^2} \quad (1)$$

In order to assess the quality of the *Fucus* spp. biomass estimation, the relative error obtained by dividing the RMSE by the estimated value, was also used, being more informative than the RMSE alone.

2.3.3. Multispectral UAV Flight

The UAV flight was performed over the *Fucus* spp. bed and surrounding area. The UAV (Matrice 210, a DJI quadcopter) was equipped with a MicaSense RedEdge sensor, with a 1.2 MP resolution, and a Zenmuse X4S sensor that captures information in the visible spectrum (RGB) with a resolution of 20 MP. The flying height was 30 m, which resulted in Ground Sampling Distances (GSD) of 2.1 cm and 0.8 cm, respectively, for the multispectral and RGB data. The along-track overlap between the consecutive images and the side-track overlap between consecutive flight lines was set to 70%. The multispectral sensor acquires data with a spectral range that includes blue (475 ± 10 nm), green (560 ± 10 nm), red (668 ± 5 nm), red-edge (717 ± 5 nm), and NIR (840 ± 20 nm) wavelengths. In-flight irradiance conditions were acquired using a Downwelling Light Sensor (DLS) mounted on top of the UAV, and images of the calibrated panels with known reflectance (Micasense, Seattle, WA, USA) were captured before the UAV flight.

Images were processed in Agisoft Mestashape software, which does the photogrammetric processing of the overlapping images, generates a digital surface model and orthorectifies the images. The final product is a mosaic of orthorectified images (individual image bands for the multispectral and RGB composite for the RGB data), precisely georeferenced by means of signalized Ground Control Points (GCP), which were surveyed with a high-precision Global Navigation Satellite System (GNSS) receiver (Spectra Precision SP60) in the real-time kinematic mode. The positional accuracy of this method is between 1 and 2 cm of the order of the image GSD. A total of 6 to 12 GCPs were used per orthomosaic. Residuals provided by the software were used as a measure of the georeferencing quality.

Additionally, the agreement between the RGB and Multispectral orthoimages allowed for positional accuracy control.

Prior to the UAV flight, training and independent validation areas were georeferenced by collecting the central coordinates of each of the 50×50 cm quadrat frames described above with the GNSS receiver. To avoid interference of the quadrats in the image classification, a circular buffer with a 0.25 m radius was drawn around each central point (using QGIS 3.16.9 tools) to delimit training and validation areas for the supervised classification procedures. The defined classes for the training ($n = 7$) and validation ($n = 3$) areas were: Sand (S); Rock, Barnacles, and Limpets (RBL); Mussels and Rock (MR); and mixture of seaweeds (AM: Algae Mixed). The QGIS SCP plugin version 7.9.4 Matera [37] was used to obtain the NDVI raster and to carry out a supervised classification of the intertidal cover based on this index (producing the files needed to feed the SWUAV_BIO plugin). Of the three available algorithms—maximum likelihood, spectral angle mapping and minimum distance—the latter performed best when applied for the supervised classification to our dataset and was therefore chosen. Indeed, the maximum likelihood method could not be applied given the small size of training and validation areas, and the spectral angle mapping algorithm misclassified some of the classes. The minimum distance algorithm has been applied successfully in other studies with training and validation areas with sizes similar to those in the present study [50] and also in other contexts [51]. To evaluate the performance of the classification per class, several metrics were used, relying on the number of correct/incorrect classifications per class: errors of commission, which result when pixels associated with a class are incorrectly identified as other classes, representing false positives; errors of omission, which occur whenever pixels that should have been identified as belonging to a particular class were simply not recognized as present, representing false negatives; recall, which is the number of correct classifications for a given class divided by the row total, including false negatives; and the f1 score, which is the harmonic mean of precision and recall measures. These metrics were calculated according to the area-based error matrix provided by the SCP plugin, where each element represents the estimated area proportion of each class. To provide a general perspective of the quality of the classification, the overall accuracy and the kappa coefficient were estimated. The overall accuracy shows the proportion of correct classifications in the total number of samples, and the kappa coefficient evaluates the performed classification, considering the possibility of an agreement occurring by chance [15].

Validation of the plugin was performed for *Fucus* spp. isolated beds, comparing the estimated in situ total biomass (g DW) for the 10 sampling quadrats with the biomass estimated for the same area by the SWUAV_BIO plugin. In situ estimation of the total biomass for the 10 *Fucus* spp. sampling quadrats was achieved by applying the obtained predictive equation that relates the percentage cover to the biomass per quadrat and summing the values obtained for all quadrats. For the application of the SWUAV_BIO plugin, the classification raster was obtained based on the UAV multispectral NDVI image for the Region of interest (ROI) for the four classes presented above. Data acquired in situ and photo interpretation of the RGB orthomosaic confirmed that the Mixed algae class matched with high precision the location and cover of the targeted *Fucus* spp. beds. Therefore, the Mixed algae class in the Vila Chã ROI classified raster, and the corresponding NDVI raster file, cropped by the polygons delineating the 10 *Fucus* spp. sampling quadrats represented *Fucus* spp. cover and could be used as such. The exact location of the 10 sampling quadrats on the *Fucus* spp. beds was defined by drawing a vector layer in QGIS with 10 polygons through photointerpretation of the RGB raster. The ROI classification raster with the class Mixed algae, the corresponding ROI NDVI raster file and the *Fucus* spp. shapefile were used as plugin input files for the validation.

2.4. Plugin Application—Case Study

For the purpose of testing the SWUAV_BIO plugin in a different context, multispectral data previously acquired from a different study area were used. This study area was located

on the rocky shore of Praia Norte (Viana do Castelo: 41°41.8'N, 8°51.1'W) in Northern Portugal, which has a sheltered upper shore with extensive beds of *Fucus* spp. and the southernmost population of *Ascophyllum nodosum* in Europe [7]. Field work and UAV (Matrice 200) flight took place on 6 June 2020 during low tide, with the definitions of training ($n = 5$) and validation ($n = 2$) areas for the classes of *Fucus* spp. and *Ascophyllum nodosum*, using the methodology described above for the plugin design and validation. Training and validation areas for Rock and Sand classes were defined in QGIS by the photointerpretation of the RGB image. Two UAV flights were performed at a 40 m height above the seaweed beds and surrounding area: the first, with the UAV equipped with a MicaSense RedEdge sensor (2.7 cm GSD), and the second equipped with a Zenmuse X4S sensor (0.9 cm GSD). The supervised classification procedures followed the methodology described above for the data used for the SWUAV_BIO plugin design and validation. The NDVI and the generated classification raster were the plugin input data for this application.

3. Results

3.1. NDVI–Seaweed Biomass Relationship

The NDVI data from the spectrometer readings were plotted against the dry biomass per unit area (g DW m^{-2}), and three regression models (Linear, Exponential, and Power) were tested (Figure 3). The models for integrating the SWUAV_BIO plugin were selected based on their fit to the data (higher R^2 and lower RMSE) (Table 1). For *Ulva* spp., the exponential model was chosen because it resulted in a markedly lower RMSE than the other models, although with a slightly lower R^2 than the next-best model. The chosen model equations were integrated into the SWUAV_BIO plugin.

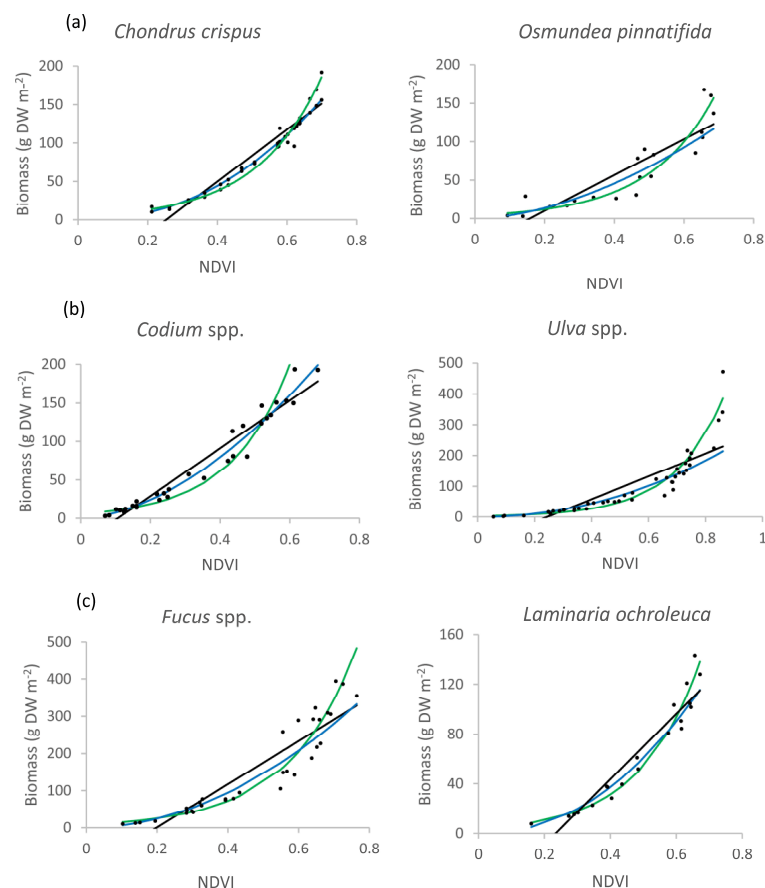


Figure 3. Tested models (Linear: black line; Exponential: green line; Power: blue line) for the relationship between NDVI and biomass for the red (a), green (b) and brown (c) seaweed.

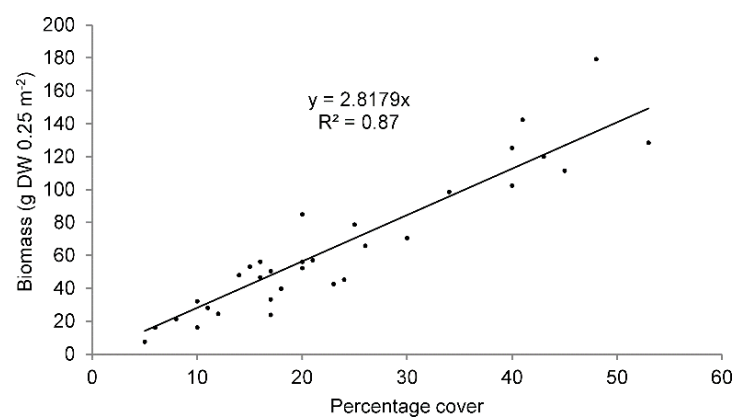
Table 1. Tested models and respective fitness for the relationship between NDVI and biomass for each seaweed species. In bold are the models integrated into the SWUAV_BIO plugin.

Species	Model	Equation	R ²	RMSE
<i>Chondrus crispus</i>	Linear	$y = 338.79 x - 85.673$	0.89	17.16
	Exponential	$y = 4.4908 e^{5.3261 x}$	0.97	8.84
	Power	$y = 351.36 \times 2.2640$	0.95	12.88
<i>Osmundea pinnatifida</i>	Linear	$y = 233.16 x - 36.700$	0.78	23.22
	Exponential	$y = 4.1340 e^{5.3085 x}$	0.84	18.87
	Power	$y = 225.08 x^{1.7403}$	0.84	21.82
<i>Codium</i> spp.	Linear	$y = 310.55 x - 33.123$	0.95	14.07
	Exponential	$y = 5.6390 e^{5.9438 x}$	0.92	29.04
	Power	$y = 397.32 x^{1.7299}$	0.98	10.77
<i>Ulva</i> spp.	Linear	$y = 370.68 x - 90.415$	0.70	55.55
	Exponential	$y = 2.7744 e^{5.7304 x}$	0.93	28.14
	Power	$y = 291.15 x^{2.0691}$	0.95	51.60
<i>Fucus</i> spp.	Linear	$y = 580.28 x - 114.880$	0.84	48.76
	Exponential	$y = 8.8671 e^{5.2320x}$	0.95	41.75
	Power	$y = 560.91 x^{1.9453}$	0.95	43.86
<i>Laminaria ochroleuca</i>	Linear	$y = 262.87 x - 61.477$	0.90	13.26
	Exponential	$y = 3.5349 e^{5.4575x}$	0.97	9.56
	Power	$y = 275.52 x^{2.1824}$	0.96	10.80

3.2. Plugin Validation

3.2.1. In Situ Data Collection

A predictive linear equation for *Fucus* spp. relating the percentage cover and the dry biomass was obtained using the percentage cover and DW data of the 32 samples (Section 2.3) (Figure 4).

**Figure 4.** Relationship between *Fucus* spp. in situ percentage cover and dry biomass per sampling quadrat ($n = 32$).

An RMSE of 15 g DW 0.25 m⁻² was obtained. Relative errors of the estimated *Fucus* spp. biomass for percentage cover of 26%, 35% and 51% were about 20%, 15% and 10%, respectively (Table 2). The relative error of the biomass estimation is smaller for higher percentage cover values, although for smaller percentage cover values, the actual individual residuals tend to be smaller.

Table 2. Relative errors of the estimated *Fucus* spp. biomass by percentages cover.

Percentage Cover (%)	Estimated Biomass (g DW 0.25 m ⁻²)	Relative Error (%)
26	73	20
35	99	15
51	144	10

3.2.2. Multispectral UAV Flight

The NDVI-based supervised classification for the Vila Chã ROI (Figure 5d) covered a total area of 11,292 m², with the Mixed algae class covering 1010 m².

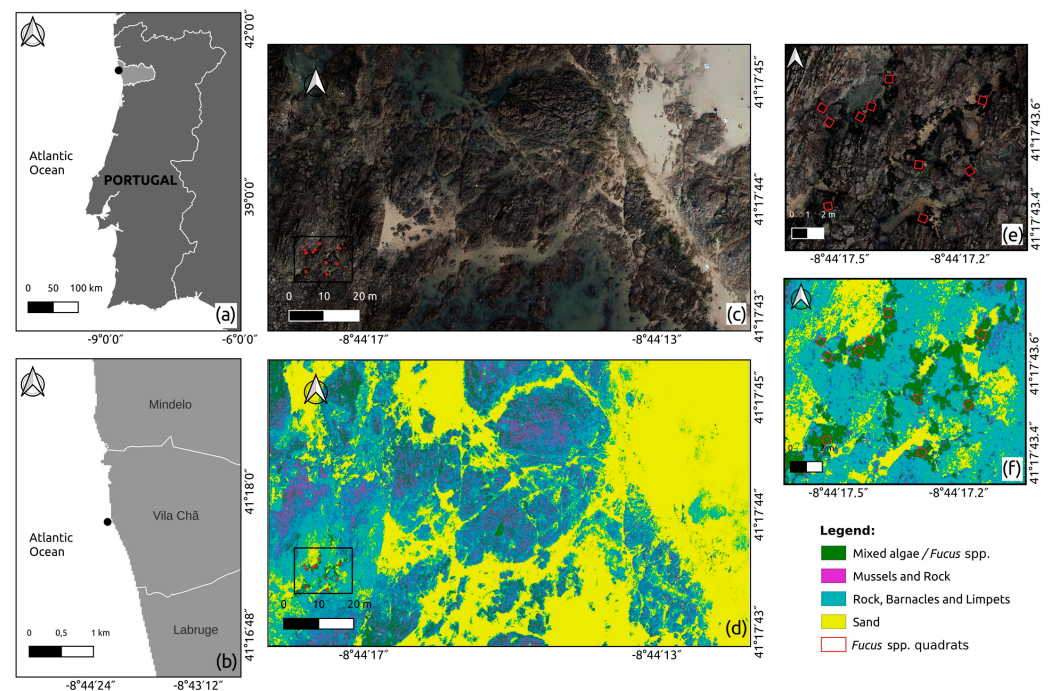


Figure 5. Vila Chã Region of Interest (ROI) maps: (a) geographical position (black dot) at Porto district in Continental Portugal and (b) detail within Vila Chã municipality coast; (c) RGB UAV retrieved raster (with inset map e); (d) supervised classification for maps with 4 classes (with inset map f); (e) location of 10 in situ sampling quadrats (red) used for the assessment of *Fucus* spp. biomass for the SWUAV_BIO plugin validation; and (f) location of 10 in situ sampling *Fucus* spp. quadrats (red).

This classification had an overall accuracy of 76.94% and a kappa coefficient of 0.65, corresponding to a good classification level of agreement [52,53]. The performance of the classification calculated from the error matrix (Table 3, adapted from [54]) indicated values ranging from low to high performance per class (Table 4). For Mixed algae, and Mussels and Rock classes, the recall was lower than precision, indicating the presence of more false negative values in the classification than false positives, as corroborated by the calculated omission and commission errors. These resulted in lower f1 scores for both classes. Higher classification performances were obtained for Rock, Barnacles and Limpets, and Sand classes with respective higher f1 scores.

Table 3. Error matrix summarising classifier performance and map accuracy of Vila Chã Region of Interest (ROI).

Thematic Map Classes	Reference Data Classes				Total
	Mixed Algae	Mussels and Rock	Rock, Barnacles and Limpets	Sand	
Mixed algae	0.04	0.03	0.02	0.00	0.09
Mussels and Rock	0.03	0.04	0.04	0.00	0.11
Rock, Barnacles and Limpets	0.05	0.06	0.21	0.00	0.32
Sand	0.00	0.00	0.00	0.48	0.48
Total	0.12	0.13	0.26	0.48	1.00

Table 4. Classification performance of Vila Chã ROI per class.

Classes	Omission Errors	Commission Errors	Precision	Recall	F1 Score
Mixed algae	0.68	0.55	0.45	0.32	0.37
Mussels and Rock	0.67	0.61	0.39	0.33	0.35
Rock, Barnacles and Limpets	0.21	0.35	0.65	0.79	0.71
Sand	0.00	0.00	1.00	1.00	1.00

For the Mixed algae class, the standard error of the area estimated by the classification was 67 m², according to the SCP output, which is an error of about 6.6% considering the total area of 1010 m².

From the application of the predictive linear equation (Figure 4) to the 10 georeferenced sampling quadrats haphazardly placed over the *Fucus* spp. beds (Figure 5e), a total biomass of 2307 g DW was estimated. Visual analysis showed high concordance between the location of *Fucus* spp. beds belonging to the Mixed algae class, as visualised in the RGB image (Figure 5e) and the correspondent classification (Figure 5f). A total biomass of 1462 g DW was estimated via the application of the SWUAV_BIO plugin workflow for the exact same area of the 10 georeferenced sampling quadrats haphazardly placed over the *Fucus* spp. beds. This is 36% less compared to the in situ assessment.

3.3. Plugin Application—Case Study

The NDVI-based supervised classification for Praia Norte (Viana do Castelo) ROI covered a total area of 37,628 m² (Figure 6c). The classification had an overall accuracy of 81.2% and a kappa coefficient of 0.65, corresponding to a good classification level of agreement [52,53]. A visual assessment confirmed that the plugin succeeded in identifying *Fucus* spp. patches.

The performance of the classification calculated from the error matrix (Table 5; adapted from [54]) indicated values ranging from low to high performance per class (Table 6). For the *Fucus* spp. class, the precision was lower than the recall, indicating the presence of more false positive values in the classification than false negatives, as corroborated by the calculated commission and omission errors, resulting in a lower f1 score. Higher classification performances were obtained for the Sand and Rock classes with respective higher f1 scores.

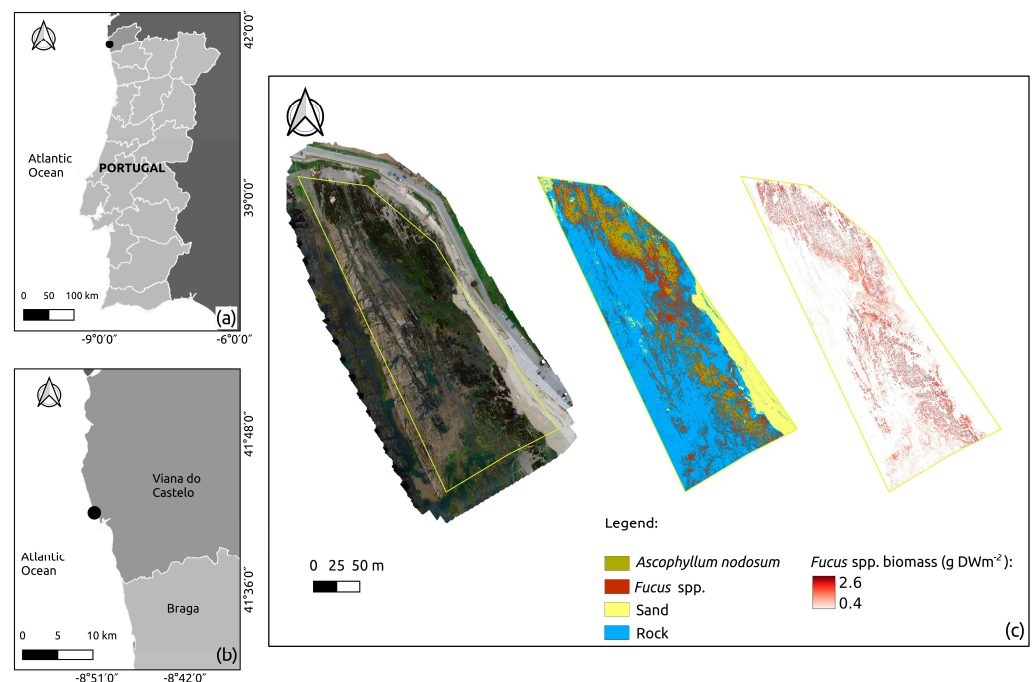


Figure 6. Praia Norte maps: (a) geographical position (black dot) at Viana do Castelo district in Continental Portugal; (b) detail within Viana do Castelo district coast; and (c) generated maps during SWUAV_BIO plugin application, from left to right: RGB raster with ROI (delimited by a yellow line); supervised classification map with 4 classes; *Fucus* spp. biomass raster.

Table 5. Error matrix summarising classifier performance and map accuracy of Praia Norte (Viana do Castelo) ROI.

Thematic Map Classes	Reference Data Classes				Total
	<i>Ascophyllum nodosum</i>	<i>Fucus</i> spp.	Sand	Rock	
<i>Ascophyllum nodosum</i>	0.04	0.03	0.02	0.00	0.09
<i>Fucus</i> spp.	0.03	0.04	0.04	0.00	0.11
Sand	0.05	0.06	0.21	0.00	0.32
Rock	0.00	0.00	0.00	0.48	0.48
Total	0.12	0.13	0.26	0.48	1.00

Table 6. Classification performance of Praia Norte (Viana do Castelo) ROI per class.

Classes	Omission Errors	Commission Errors	Precision	Recall	F1 Score
<i>Ascophyllum nodosum</i>	0.43	0.42	0.58	0.57	0.58
<i>Fucus</i> spp.	0.39	0.72	0.28	0.61	0.39
Sand	0.00	0.00	1.00	1.00	1.00
Rock	0.16	0.00	1.00	0.84	0.91

The area covered by the *Fucus* spp. class was 7882 m², with a total biomass estimated by the SWUAV_BIO plugin of 12,562,846 g DW (about 12,563 kg DW). The error associated with the biomass-NDVI model was 41.75 g DW m⁻² (ca. 2.6% of the total *Fucus* spp. biomass), and the classification standard error for the area estimate of this cover class was 139 m², according to the SCP output, being about 1.8%.

4. Discussion

This study combined field surveys and high-resolution multispectral UAV imagery to develop a new methodology to remotely map and quantify intertidal seaweed biomass from different groups. Seaweed biomass–NDVI relationships were parameterized and integrated in a QGIS plugin to allow expedited biomass estimation from multispectral survey data. The species percentage cover–biomass relationship was used for validation of the method in terms of *Fucus* spp. biomass estimation. At Vila Chã, the *Fucus* spp. biomass estimated with the proposed method through the SWUAV_BIO plugin was underestimated by 36% compared to the in situ assessment.

Despite the presence of false negatives in the classification of the whole ROI, indicating that pixels belonging to the Mixed algae class were attributed to other classes, there was a high visual concordance between the location of *Fucus* spp. beds belonging to the Mixed algae class in the RGB image and the correspondent classification (Figure 5e,f). The issues associated with false negative and false positive values in the Mixed algae mixed class could reflect its heterogeneity and lack of pureness. The spectral signatures can be contaminated due to the low cover of annual seaweeds during less favourable seasons. During the survey in December, most of the annual seaweeds presented low abundance and percentage cover, and most of the training and validation areas had abundant substrate cover. Such was not the case for the *Fucus* spp. beds that comprehend perennial seaweeds and, therefore, maintained a high abundance and percentage cover in December. However, the saturation of the NDVI values when a certain biomass is reached suggests that there may be a limit to the detection of higher biomass values when a certain thickness of cover is reached [42,55,56].

Other studies have demonstrated that the spectral reflectance can be influenced by plant water stress (e.g., [57,58]), and it is possible that dehydration due to emersion during low tide would also affect the spectral patterns of *Fucus* spp. and hence influence the NDVI-based biomass estimation. Additionally, inter and intraspecific seaweed spectral differences in response to physiological or seasonal changes have also been reported since reflectance is ruled by physical and physiological parameters that can vary for a species or even within an individual over space and time [36,59]. Previous authors have reported a multifaceted relationship between salinity, temperature and pigment concentration for the brown seaweed *Fucus vesiculosus* [60]. Specifically, reduced salinity mostly increased the pigment concentration of *F. vesiculosus* at normal ambient temperature, whereas elevated temperature reversed the effect [60]. Moreover, the same authors reported that differences in Chlorophyll *a* and *b* concentrations resulted in a consistent change of spectral reflectance for *F. vesiculosus*. Furthermore, changes in the physiological condition of giant kelp (*Macrocystis pyrifera*) canopy, expressed in terms of the reflectance and transmittance of these kelp fronds, have been used to assess their spectral variability for providing insights into their ecology and biophysiology using remote sense tools (see [61]). Therefore, it is expected that intertidal seaweed UAV biomass estimations for the same location will vary according to the low tide level and emersion interval at the time of the flight, as well as with seaweed physiological and ontogenic states. In this sense, the total *Fucus* spp. biomass assessed for Praia Norte (Viana do Castelo) is likely to also be an underestimation of the real available biomass.

In opposition to these findings, there were also false positive values in the classification, indicating that pixels belonging to other classes (*Ascophyllum nodosum* and Rock classes) were being classified as *Fucus* spp. class. Both *A. nodosum* and *Fucus* spp. are Fucales, occurring interspersed at Praia Norte. It is consequently likely that their distinction by the proposed workflow has limitations. The several steps required to implement the SWUAV_BIO plugin procedures presented in this study generate residual errors that will have a cumulative effect, which is reflected in the underestimated *Fucus* spp. total biomass values. These errors are related to in situ biomass estimation, the NDVI-to-biomass estimation and the classification process (e.g., the error of the estimated area for the target class) and should be considered when interpreting the SWUAV_BIO outputs. Therefore,

despite the fact that supervised classifications for both Vila Chã and Praia Norte presented general accuracy metrics with good levels of agreement, the inspection of the classification performance by class, combined with the photointerpretation of the RGB imagery and knowledge of the terrain, was essential for data interpretation.

The remote estimation of intertidal seaweed biomass presents several challenges. In rocky shores, that task is particularly difficult due to different sources of noise in the reflectance spectra, such as sun glint from rock pools surfaces and shade due to microtopography and the angle of incident sunlight. Less favourable conditions are found in late autumn and early winter when the sun elevation is lower and generates large shadow areas (areas without direct sunlight). Ideally, these areas should be masked and eliminated from the classification. Previous tests indicated that, at least in periods of higher sun elevation, the proportion of shadows is relatively small, not having a significant impact. Future work will consider the delimitation of shadow areas based on the high-resolution 3D model obtained, photogrammetric processing and the precise time of image acquisition.

Intertidal hydrodynamics also affects biological assemblages. Surf zone hydrodynamics vary from narrow, more reflective surf zones to wide and more dissipative surf zones [25]. For instance, in the northwest of Portugal, sheltered shores, such as Praia Norte (Viana do Castelo) with dissipative surf zones due to gradually sloping bottoms and waves breaking far from shore [25], allow the recruitment and development of extensive seaweed assemblages dominated by *Fucus* spp. and *A. nodosum*. On more exposed shores, with surf zones characterized by steeper slopes, considered more reflective, waves break closer to the shore, and seaweed assemblages are characterized by a mixture of red and green seaweed occurring more abundantly along a narrow strip at the low shore level. In the latter case, the described methodology would not be applicable, given the high degree of seaweed mixture that would make it impossible to discriminate reflectance by taxon.

Nonetheless and although the SWUAV_BIO plugin tends to underestimate biomass (compared to field data), this plugin is a valuable tool as it provides an expedited means for seaweed standing stock assessments, which is useful for seaweed population monitoring and resource management, such as following the seasonal and yearly fluctuations of seaweed abundance and assessing the effects of harvesting. In this context, the generated conservative measures, integrated with local knowledge of seaweed abundances, are advantageous as they promote the cautious management of these resources.

Additionally, the development of such a plugin in open-source GIS software provides several benefits. The software is open-source and free, making the code available to any user/developer to modify and adapt it to other specific needs. It provides components or tools that can be used in other contexts and areas, having the NDVI and classification maps as baselines, with the possibility to integrate new equations for the biomass/NDVI relationship of other species. For studies conducted during different seasons of the year, particular attention should be given to the potential effects of the phenology of the seaweeds under study. It is recommended that in situ biomass estimations and NDVI to biomass estimations encompass changes such as reproductive status and senescence. One of the main advantages of the plugin is the low computer processing power required, which allows the plugin to be easily operated in different computer environments, replacing manual procedures that would require time to process. Furthermore, there are no limitations to the dissemination of this tool in terms of licenses, and it includes support documentation to assist the user (the SWUAV_BIO plugin contains a tutorial explaining the plugin and its use).

5. Conclusions

In this work, a methodology was developed and validated to quantify intertidal seaweed biomass based on multispectral imagery acquired with a UAV that was made freely available through an easy-to-use QGIS plugin. The SWUAV_BIO plugin is able to assess with considerable accuracy the biomass of intertidal seaweed beds using multispectral data collected by a UAV. The plugin includes equations for *Fucus* spp. (validated in this

study) and other seaweeds (requiring additional validation), leaving room for further investigation, with validation and application studies directed to other seaweed species or groups. SWUAV_BIO can therefore be a valuable tool to map and quantify the biomass of intertidal seaweeds, as well as an incentive for the development of new research on monospecific seaweed beds and further research on seaweed biomass estimation. By providing increased knowledge on coastal habitats, its application will contribute to the sustainable management and conservation of marine ecosystems, as well as the sustainable use of wild seaweeds.

Author Contributions: Conceptualisation, D.B. and J.A.G.; methodology, D.B., I.C., J.S., L.D., A.B. and J.A.G.; software, L.D. and D.B.; validation, D.B., I.C., J.S., L.D., A.B., I.S.-P. and J.A.G.; formal analysis, D.B., A.B. and J.A.G.; investigation, D.B., I.C., J.S., L.D., A.B., I.S.-P. and J.A.G.; resources I.S.-P. and J.A.G.; data curation, D.B.; writing, original draft preparation, D.B.; writing, review and editing, D.B., L.D., I.C., A.B., J.S., I.S.-P. and J.A.G.; visualisation, D.B., I.C., J.S., L.D., A.B., I.S.-P. and J.A.G.; project administration D.B. and J.A.G.; funding acquisition, D.B., I.C., I.S.-P. and J.A.G. All authors have read and agreed to the published version of the manuscript.

Funding: The research leading to these results has received funding from the EEA Grants 2014–2021. This work was funded by BlueForestry (PT-INNOVATION-0077) and SWUAV (POCI-01-0145-FEDER-032233) and supported by the POCI and FCT, Foundation for Science and Technology, through OE, and partially by UIDB/04423/2020, UIDB/04683/2020, UIDP/04423/2020 and UIDP/04683/2020 supported by national funds through FCT.

Data Availability Statement: The datasets in this study are available from the corresponding author upon reasonable request.

Acknowledgments: We thank Isabel Gómez and Rosa Melo for assistance during field work. Our thanks go also to Luís Pádua for his advice on the use of the accuracy metrics. We are grateful to the two anonymous reviewers for their constructive comments on this manuscript.

Conflicts of Interest: The authors declare no conflict of interest.

References

1. Girão, M.; Ribeiro, I.; Ribeiro, T.; Azevedo, I.C.; Pereira, F.; Urbatzka, R.; Leão, P.N.; Carvalho, M.F. Actinobacteria Isolated From *Laminaria ochroleuca*: A Source of New Bioactive Compounds. *Front. Microbiol.* **2019**, *10*, 683. [\[CrossRef\]](#)
2. Hafting, J.T.; Craigie, J.S.; Stengel, D.B.; Loureiro, R.R.; Buschmann, A.H.; Yarish, C.; Edwards, M.D.; Critchley, A.T. Prospects and challenges for industrial production of seaweed bioactives. *J. Phycol.* **2015**, *51*, 821–837. [\[CrossRef\]](#)
3. Cotas, J.; Pacheco, D.; Gonçalves, A.M.M.; Silva, P.; Carvalho, L.G.; Pereira, L. Seaweeds' nutraceutical and biomedical potential in cancer therapy: A concise review. *J. Cancer Metastasis Treat.* **2021**, *7*, 13. [\[CrossRef\]](#)
4. López-Hortas, L.; Flórez-Fernández, N.; Torres, M.D.; Ferreira-Anta, T.; Casas, M.P.; Balboa, E.M.; Falqué, E.; Domínguez, H. Applying Seaweed Compounds in Cosmetics, Cosmeceuticals and Nutricosmetics. *Mar. Drugs* **2021**, *19*, 552. [\[CrossRef\]](#) [\[PubMed\]](#)
5. Underwood, A.J. Experimental ecology of rocky intertidal habitats: What are we learning? *J. Exp. Mar. Biol. Ecol.* **2000**, *250*, 51–76. [\[CrossRef\]](#) [\[PubMed\]](#)
6. Murfitt, S.L.; Allan, B.M.; Bellgrove, A.; Rattray, A.; Young, M.A.; Ierodiaconou, D. Applications of unmanned aerial vehicles in intertidal reef monitoring. *Sci. Rep.* **2017**, *7*, 10259. [\[CrossRef\]](#) [\[PubMed\]](#)
7. Borges, D.; Araujo, R.; Azevedo, I.; Pinto, I.S. Sustainable management of economically valuable seaweed stocks at the limits of their range of distribution: *Ascomyllum nodosum* (Phaeophyceae) and its southernmost population in Europe. *J. Appl. Phycol.* **2020**, *32*, 1365–1375. [\[CrossRef\]](#)
8. Melo, R.; Sousa-Pinto, I.; Antunes, S.C.; Costa, I.; Borges, D. Temporal and spatial variation of seaweed biomass and assemblages in Northwest Portugal. *J. Sea Res.* **2021**, *174*, 102079. [\[CrossRef\]](#)
9. Candiago, S.; Remondino, F.; De Giglio, M.; Dubbini, M.; Gattelli, M. Evaluating Multispectral Images and Vegetation Indices for Precision Farming Applications from UAV Images. *Remote Sens.* **2015**, *7*, 4026–4047. [\[CrossRef\]](#)
10. Torres-Sánchez, J.; López-Granados, F.; Serrano, N.; Arquero, O.; Peña, J.M. High-Throughput 3-D Monitoring of Agricultural-Tree Plantations with Unmanned Aerial Vehicle (UAV) Technology. *PLoS ONE* **2015**, *10*, e0130479. [\[CrossRef\]](#)
11. Honrado, J.L.E.; Solpico, D.B.; Favila, C.M.; Tongson, E.; Tangonan, G.L.; Libatique, N.J.C. UAV imaging with low-cost multispectral imaging system for precision agriculture applications. In Proceedings of the 2017 IEEE Global Humanitarian Technology Conference (GHTC), San Jose, CA, USA, 19–22 October 2017; pp. 1–7.
12. Soubry, I.; Patias, P.; Tsioukas, V. Monitoring vineyards with UAV and multi-sensors for the assessment of water stress and grape maturity. *J. Unmanned Veh. Syst.* **2017**, *5*, 37–50. [\[CrossRef\]](#)

13. López-García, P.; Intrigliolo, D.S.; Moreno, M.A.; Martínez-Moreno, A.; Ortega, J.F.; Pérez-Álvarez, E.P.; Ballesteros, R. Assessment of Vineyard Water Status by Multispectral and RGB Imagery Obtained from an Unmanned Aerial Vehicle. *Am. J. Enol. Vitic.* **2021**, *72*, 285–297. [\[CrossRef\]](#)
14. Devia, C.A.; Rojas, J.P.; Petro, E.; Martinez, C.; Mondragon, I.F.; Patino, D.; Rebolledo, M.C.; Colorado, J. High-Throughput Biomass Estimation in Rice Crops Using UAV Multispectral Imagery. *J. Intell. Robot. Syst.* **2019**, *96*, 573–589. [\[CrossRef\]](#)
15. Borges, D.; Padua, L.; Azevedo, I.C.; Silva, J.; Sousa, J.J.; Sousa-Pinto, I.; Gonçalves, J.A. Classification of an Intertidal Reef by Machine Learning Techniques Using UAV Based RGB and Multispectral Imagery. In Proceedings of the 2021 IEEE International Geoscience and Remote Sensing Symposium IGARSS, Brussels, Belgium, 11–16 July 2021; pp. 64–67.
16. Collin, A.; Dubois, S.; James, D.; Houet, T. Improving Intertidal Reef Mapping Using UAV Surface, Red Edge, and Near-Infrared Data. *Drones* **2019**, *3*, 67. [\[CrossRef\]](#)
17. Van der Wal, D.; van Dalen, J.; Wielemaker-van den Dool, A.; Dijkstra, J.T.; Ysebaert, T. Biophysical control of intertidal benthic macroalgae revealed by high-frequency multispectral camera images. *J. Sea Res.* **2014**, *90*, 111–120. [\[CrossRef\]](#)
18. Brodie, J.; Ash, L.V.; Tittley, I.; Yesson, C. A comparison of multispectral aerial and satellite imagery for mapping intertidal seaweed communities. *Aquat. Conserv.* **2018**, *28*, 872–881. [\[CrossRef\]](#)
19. Taddia, Y.; Russo, P.; Lovo, S.; Pellegrinelli, A. Multispectral UAV monitoring of submerged seaweed in shallow water. *Appl. Geomat.* **2020**, *12*, 19–34. [\[CrossRef\]](#)
20. Tait, L.; Bind, J.; Charan-Dixon, H.; Hawes, I.; Pirker, J.; Schiel, D. Unmanned Aerial Vehicles (UAVs) for Monitoring Macroalgal Biodiversity: Comparison of RGB and Multispectral Imaging Sensors for Biodiversity Assessments. *Remote Sens.* **2019**, *11*, 2332. [\[CrossRef\]](#)
21. Rossiter, T.; Furey, T.; McCarthy, T.; Stengel, D.B. Application of multiplatform, multispectral remote sensors for mapping intertidal macroalgae: A comparative approach. *Aquat. Conserv.* **2020**, *30*, 1595–1612. [\[CrossRef\]](#)
22. Bell, T.W.; Nidzieko, N.J.; Siegel, D.A.; Miller, R.J.; Cavanaugh, K.C.; Nelson, N.B.; Reed, D.C.; Fedorov, D.; Moran, C.; Snyder, J.N.; et al. The Utility of Satellites and Autonomous Remote Sensing Platforms for Monitoring Offshore Aquaculture Farms: A Case Study for Canopy Forming Kelps. *Front. Mar. Sci.* **2020**, *7*, 520223. [\[CrossRef\]](#)
23. Cavanaugh, K.C.; Cavanaugh, K.C.; Bell, T.W.; Hockridge, E.G. An Automated Method for Mapping Giant Kelp Canopy Dynamics from UAV. *Front. Environ. Sci.* **2021**, *8*, 587354. [\[CrossRef\]](#)
24. Saccomanno, V.R.; Bell, T.; Pawlak, C.; Stanley, C.K.; Cavanaugh, K.C.; Hohman, R.; Klausmeyer, K.R.; Cavanaugh, K.; Nickels, A.; Hewerdine, W.; et al. Using unoccupied aerial vehicles to map and monitor changes in emergent kelp canopy after an ecological regime shift. *Remote Sens. Ecol. Conserv.* **2022**, *9*, 62–75. [\[CrossRef\]](#)
25. Conser, E.; Shanks, A.L. Density of benthic macroalgae in the intertidal zone varies with surf zone hydrodynamics. *Phycologia* **2019**, *58*, 254–259. [\[CrossRef\]](#)
26. Chen, J.; Li, X.; Wang, K.; Zhang, S.; Li, J. Estimation of Seaweed Biomass Based on Multispectral UAV in the Intertidal Zone of Gouqi Island. *Remote Sens.* **2022**, *14*, 2143. [\[CrossRef\]](#)
27. Praeger, C.; Vucko, M.J.; McKinna, L.; de Nys, R.; Cole, A. Estimating the biomass density of macroalgae in land-based cultivation systems using spectral reflectance imagery. *Algal. Res.* **2020**, *50*, 102009. [\[CrossRef\]](#)
28. Che, S.; Du, G.; Wang, N.; He, K.; Mo, Z.; Sun, B.; Chen, Y.; Cao, Y.; Wang, J.; Mao, Y. Biomass estimation of cultivated red algae *Pyropia* using unmanned aerial platform based multispectral imaging. *Plant Methods* **2021**, *17*, 12. [\[CrossRef\]](#) [\[PubMed\]](#)
29. Hu, L.; Hu, C.; Ming-Xia, H.E. Remote estimation of biomass of *Ulva prolifera* macroalgae in the Yellow Sea. *Remote Sens. Environ.* **2017**, *192*, 217–227. [\[CrossRef\]](#)
30. Karki, S.; Bermejo, R.; Wilkes, R.; Monagail, M.M.; Daly, E.; Healy, M.; Hanafin, J.; McKinsty, A.; Mellander, P.-E.; Fenton, O.; et al. Mapping Spatial Distribution and Biomass of Intertidal *Ulva* Blooms Using Machine Learning and Earth Observation. *Front. Mar. Sci.* **2021**, *8*, 633128. [\[CrossRef\]](#)
31. Kriegler, F.J.; Malila, W.A.; Nalepka, R.F.; Richardson, W. Preprocessing Transformations and Their Effects on Multispectral Recognition. In Proceedings of the Remote Sensing of Environment, VI, Ann Arbor, MI, USA, 1 January 1969; p. 97.
32. Rouse, J.W., Jr.; Haas, R.H.; Schell, J.A.; Deering, D.W. Monitoring Vegetation Systems in the Great Plains with ERTS. In *NASA Special Publication*; NASA: Washington, DC, USA, 1974; Volume 351, p. 309.
33. Tucker, C.J. Red and photographic infrared linear combinations for monitoring vegetation. *Remote Sens. Environ.* **1979**, *8*, 127–150. [\[CrossRef\]](#)
34. Jensen, J.R. *Introductory Digital Image Processing: A Remote Sensing Perspective*; Prentice Hall, Inc.: Hoboken, NJ, USA, 1986.
35. Tucker, C.J.; Sellers, P.J. Satellite remote sensing of primary production. *Int. J. Remote Sens.* **1986**, *7*, 1395–1416. [\[CrossRef\]](#)
36. Chao Rodríguez, Y.; Domínguez Gómez, J.A.; Sánchez-Carnero, N.; Rodríguez-Pérez, D. A comparison of spectral macroalgae taxa separability methods using an extensive spectral library. *Algal. Res.* **2017**, *26*, 463–473. [\[CrossRef\]](#)
37. Congedo, L. Semi-Automatic Classification Plugin: A Python tool for the download and processing of remote sensing images in QGIS. *J. Open Source Softw.* **2021**, *6*, 3172. [\[CrossRef\]](#)
38. Arekhi, M.; Goksel, C.; Balik Sanli, F.; Senel, G. Comparative Evaluation of the Spectral and Spatial Consistency of Sentinel-2 and Landsat-8 OLI Data for Igneada Longos Forest. *ISPRS Int. J. Geo-Inf.* **2019**, *8*, 56. [\[CrossRef\]](#)
39. Oddi, L.; Cremonese, E.; Ascari, L.; Filippa, G.; Galvagno, M.; Serafino, D.; Cella, U.M.d. Using UAV Imagery to Detect and Map Woody Species Encroachment in a Subalpine Grassland: Advantages and Limits. *Remote Sens.* **2021**, *13*, 1239. [\[CrossRef\]](#)

40. Myers, D.J.; Schweik, C.M.; Wicks, R.; Bowlick, F.; Carullo, M. Developing a land cover classification of salt marshes using UAS time-series imagery and an open source workflow. *Int. Arch. Photogramm. Remote Sens. Spat. Inf. Sci.* **2018**, *XLII-4/W8*, 155–162. [CrossRef]
41. Smyth, T.A.G.; Wilson, R.; Rooney, P.; Yates, K.L. Extent, accuracy and repeatability of bare sand and vegetation cover in dunes mapped from aerial imagery is highly variable. *Aeolian Res.* **2022**, *56*, 100799. [CrossRef]
42. Barillé, L.; Robin, M.; Harin, N.; Bargain, A.; Launeau, P. Increase in seagrass distribution at Bourgneuf Bay (France) detected by spatial remote sensing. *Aquat. Bot.* **2010**, *92*, 185–194. [CrossRef]
43. QGIS.org. QGIS 3.16. Geographic Information System Installation Guide. QGIS Association. Available online: <https://github.com/qgis/QGIS/blob/master/INSTALL.md> (accessed on 31 March 2020).
44. GDAL/OGR, c. GDAL/OGR Geospatial Data Abstraction software Library. Open Source Geospatial Foundation. Available online: <https://gdal.org/> (accessed on 31 March 2020).
45. Conrad, O.; Bechtel, B.; Bock, M.; Dietrich, H.; Fischer, E.; Gerlitz, L.; Wehberg, J.; Wichmann, V.; Böhner, J. System for Automated Geoscientific Analyses (SAGA) v. 2.1.4. *Geosci. Model Dev.* **2015**, *8*, 1991–2007. [CrossRef]
46. GRASS Development Team. Geographic Resources Analysis Support System (GRASS) Software, Version 7.8. Open Source Geospatial Foundation. Available online: <https://grass.osgeo.org/> (accessed on 31 March 2020).
47. Van Rossum, G.; Drake, F.L. *Python 3 Reference Manual*; CreateSpace: Scotts Valley, CA, USA, 2009; Available online: <https://www.python.org/> (accessed on 31 March 2020).
48. PyQt, 2012. PyQt Reference Guide. Available online: <https://doc.qt.io/qtforpython/> (accessed on 31 March 2020).
49. QGIS.org, 2020. QGIS 3.16. Geographic Information System API Documentation. QGIS Association. Available online: <https://api.qgis.org/api/> (accessed on 31 March 2020).
50. Hoang, T.C.; O’Leary, M.J.; Fotedar, R.K. Remote-Sensed Mapping of Sargassum spp. Distribution around Rottnest Island, Western Australia, Using High-Spatial Resolution WorldView-2 Satellite Data. *J. Coast. Res.* **2016**, *32*, 1310–1321, 1312.
51. Hoang, T.; Garcia, R.; O’Leary, M.; Fotedar, R. Identification and Mapping of Marine Submerged Aquatic Vegetation in Shallow Coastal Waters with WorldView-2 Satellite Data. *J. Coast. Res.* **2016**, *75*, 1287–1291, 1285. [CrossRef]
52. Landis, J.R.; Koch, G.G. The measurement of observer agreement for categorical data. *Biometrics* **1977**, *33*, 159–174. [CrossRef]
53. Richards, J.A. *Remote Sensing Digital Image Analysis: An Introduction*; Springer: Berlin/Heidelberg, Germany, 2012.
54. Congalton, R.G.; Green, K. *Assessing the Accuracy of Remotely Sensed Data: Principles and Practices*; Press, C., Ed.; CRC Press: Boca Raton, FL, USA, 2008. [CrossRef]
55. Tucker, C.J. Asymptotic nature of grass canopy spectral reflectance. *Appl. Opt.* **1977**, *16*, 1151–1156. [CrossRef] [PubMed]
56. Gao, X.; Huete, A.R.; Ni, W.; Miura, T. Optical-biophysical relationships of vegetation spectra without background contamination. *Remote Sens. Environ.* **2000**, *74*, 609–620. [CrossRef]
57. Zhang, L.; Zhang, H.; Niu, Y.; Han, W. Mapping Maize Water Stress Based on UAV Multispectral Remote Sensing. *Remote Sens.* **2019**, *11*, 605. [CrossRef]
58. Gutierrez, M.; Reynolds, M.P.; Klatt, A.R. Association of water spectral indices with plant and soil water relations in contrasting wheat genotypes. *J. Exp. Bot.* **2010**, *61*, 3291–3303. [CrossRef]
59. Fyfe, S.K. Spatial and temporal variation in spectral reflectance: Are seagrass species spectrally distinct? *Limnol. Oceanogr.* **2003**, *48*, 464–479. [CrossRef]
60. Vahtmäe, E.; Kotta, J.; Orav-Kotta, H.; Kotta, I.; Pärnoja, M.; Kutser, T. Predicting macroalgal pigments (chlorophyll a, chlorophyll b, chlorophyll a + b, carotenoids) in various environmental conditions using high-resolution hyperspectral spectroradiometers. *Int. J. Remote Sens.* **2018**, *39*, 5716–5738. [CrossRef]
61. Bell, T.W.; Cavanaugh, K.C.; Siegel, D.A. Remote monitoring of giant kelp biomass and physiological condition: An evaluation of the potential for the Hyperspectral Infrared Imager (HyspIRI) mission. *Remote Sens. Environ.* **2015**, *167*, 218–228. [CrossRef]

Disclaimer/Publisher’s Note: The statements, opinions and data contained in all publications are solely those of the individual author(s) and contributor(s) and not of MDPI and/or the editor(s). MDPI and/or the editor(s) disclaim responsibility for any injury to people or property resulting from any ideas, methods, instructions or products referred to in the content.